COMMUN. MATH. SCI.
Vol. 13, No. 5, pp. 1135–1161

TOPOLOGY PRESERVATION FOR IMAGE-REGISTRATION-RELATED DEFORMATION FIELDS*

SOLÈNE OZERÉ† AND CAROLE LE GUYADER‡

Abstract. In this paper, we address the issue of designing a theoretically well-motivated and computationally efficient method ensuring topology preservation on image-registration-related deformation fields. The model is motivated by a mathematical characterization of topology preservation for a deformation field mapping two subsets of $\mathbb{Z}^2$, namely, positivity of the four approximations to the Jacobian determinant of the deformation on a square patch. The first step of the proposed algorithm thus consists in correcting the gradient vector field of the deformation (that does not comply with the topology preservation criteria) at the discrete level in order to fulfill this positivity condition. Once this step is achieved, it thus remains to reconstruct the deformation field, given its full set of discrete gradient vectors. We propose to decompose the reconstruction problem into independent problems of smaller dimensions, yielding a natural parallelization of the computations and enabling us to reduce drastically the computational time (up to 80 in some applications). For each subdomain, a functional minimization problem under Lagrange interpolation constraints is introduced and its well-posedness is studied: existence/uniqueness of the solution, characterization of the solution, convergence of the method when the number of data increases to infinity, discretization with the Finite Element Method and discussion on the properties of the matrix involved in the linear system. Numerical simulations based on OpenMP parallelization and MKL multi-threading demonstrating the ability of the model to handle large deformations (contrary to classical methods) and the interest of having decomposed the problem into smaller ones are provided.

Key words. D^m-splines, constrained optimization, variational formulation, convergence, finite element method, image registration.

AMS subject classifications. 41A15, 65D05, 65D07, 65D10, 65K10, 65Y05, 68U10.

1. Introduction

Given two images called Template and Reference, registration consists in determining an optimal diffeomorphic transformation φ such that the deformed Template image is aligned with the Reference. This technique is encountered in a wide range of fields, such as medical imaging, when comparing data to a common Reference frame, when fusing images that have not necessarily been acquired through similar sensors, or when tracking shapes. For images of the same modality, the goal of registration is to correlate the geometrical features and the intensity level distribution of the Reference and those of the Template. For images produced by different mechanisms and possessing distinct modalities, the goal of registration is to correlate the images while maintaining the modality of the Template. For an extensive overview of existing parametric and non-parametric registration methods, we refer the reader to the work by Modersitzki [28] and [29].

Generally, a physical interpretation is given to the problem of registration: the shapes to be matched are considered to be the observations of a body subjected to deformations. The deformation must thus remain physically and mechanically meaningful, and reflect material properties: self-penetration of the matter (indicating that the transformation is not injective, which is not physically consistent) should be prohibited.

*Received: April 30, 2014; accepted (in revised form): July 5, 2014. Communicated by Luminita Vese.

†Normandie Université, Laboratoire de Mathématiques de l'INSA de Rouen, 685 Avenue de l'Université BP08, 76801 Saint-Etienne-du-Rouvray Cedex, France (solene.ozere@insa-rouen.fr).

‡Normandie Université, Laboratoire de Mathématiques de l'INSA de Rouen, 685 Avenue de l'Université BP08, 76801 Saint-Etienne-du-Rouvray Cedex, France (carole.le-guyader@insa-rouen.fr).

Mathematically, topology preservation (or orientation preservation) for a deformation field mapping two subdomains of $\mathbb{Z}^2$ can be expressed by the following equivalent statements (see [25] for further details): positivity of the four approximations to the Jacobian determinant of the deformation on a square patch, corresponding angles of the deformed configuration between 0 and π, or positivity of the signed areas of triangles defined on the deformed configuration. When any of these characterizations is violated, the convexity of the deformed region is infringed, signifying that the images of the corner points of a square patch cross over the diagonal connecting their neighbors. Visually, the deformation field exhibits overlaps (see Figure 1.1 for such an example). This currently occurs when dealing with problems involving large magnitude deformations.

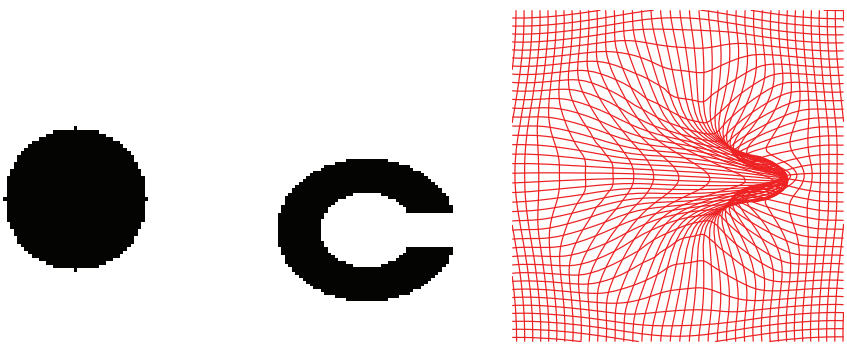

Fig. 1.1: *Academic example: Registration of a black disk to the letter C without topology-preserving conditions. From left to right: Template image, Reference image and deformation field. The deformation map clearly exhibits overlaps.*

The necessity of preserving topology arises in brain mapping for instance. It is well-known that the cortical surface has a spherical topology (i.e., is homeomorphic to the sphere or equivalently, the cortical surface has genus zero), so throughout the registration process, this feature must be preserved. This medical illustration, among others, constitutes a motivation for our work. We refer the reader to [23] and [24] for further discussion about this anatomical property. Generally speaking, as soon as the shapes to be correlated are homeomorphic, the preservation of orientation must be ensured.

The main goal of the paper is thus to design a theoretically well-motivated and computationally efficient method taking as input the deformation field that does not comply with the topology preservation criteria, and giving as output, a corrected version of this deformation, as faithful as possible to the original one.

Prior related works addressed this question of maintaining topology. In variational frameworks, the main idea is to control the Jacobian determinant of the deformation, proper measure for the local volume transformation under the considered deformation. We would like to mention the work by Ashburner et al. (see [5, 6] and [7]) and the work by Musse et al. (see [30]). In [30], the deformation map is modeled as a hierarchical displacement field decomposed on a multiresolution B-splines basis. Topology preservation is enforced by controlling the Jacobian of the transformation. The problem amounts to solving a constrained optimization problem: the residual energy between the target and the deformed source image is minimized under constraints on the Jacobian. This paper is then extended to the 3D case by Noblet et al. (see [32]). The main difference with the proposed approach is that, in our case, the set of feasible transformations is

not restricted to a certain class of mappings.
In [14] (work dedicated to registration under nonlinear elasticity principles), Droske and Rumpf address the issue of non-rigid registration of multi-modal image data. A suitable deformation is determined *via* the minimization of a morphological matching functional which locally measures the defect of the normal fields of the set of level lines of the Template image and the deformed Reference image. The matching criterion includes first order derivatives of the deformation and is complemented by a nonlinear elastic regularization of the form $\int_\Omega W(D\Phi, \mathrm{Cof}\, D\Phi, \det D\Phi)\,\mathrm{d}x$, where $W : \mathbb{R}^{3\times3} \times \mathbb{R}^{3\times3} \times \mathbb{R} \to \mathbb{R}$ is supposed to be convex, $D\Phi$ is the Jacobian matrix of the deformation Φ, $\mathrm{Cof}\, D\Phi$, the cofactor matrix of $D\Phi$ and $\det D\Phi$, the Jacobian determinant.

In [27], Le Guyader and Vese introduce a non-parametric combined segmentation/registration model in which the shapes to be matched are viewed as Ciarlet–Geymonat materials. The stored energy function of such a material is built so that it becomes infinite when the Jacobian determinant of the deformation tends to 0^+. In [21], Haber and Modersitzki address the issue of non-parametric image registration under volume-preserving constraints. They propose to restrict the set of feasible mappings by adding a volume-preserving constraint which forces the Jacobian of the deformation to be equal to 1. In [22], the authors pursue in the same direction: they propose to keep the Jacobian determinant bounded, which leads to an inequality-constrained minimization problem.

An information-theoretic-based approach is proposed in [34] to generate diffeomorphic mappings and to monitor the statistical distribution of the Jacobian determinant. The authors propose to quantify the magnitude of the deformation by means of the Kullback–Leibler distance between the probability density function associated with the deformation and the identity mapping.

Although theoretically well-motivated, the above mentioned models are hard to handle numerically, requiring for instance, the use of optimization techniques such as logarithmic barrier methods or special discretization schemes (see [33] or [29]). This observation led us to disconnect the registration problem from the topology-preserving question.

An alternative to the straight penalization of the Jacobian of the deformation was proposed by Christensen and collaborators. In [11], they introduce a viscous fluid registration model in which objects are viewed as fluids evolving in accordance with the fluid dynamics Navier–Stokes equations. This model is complemented by a regridding technique ensuring positivity of the Jacobian determinant. The method consists in monitoring the values of the Jacobian determinant of the deformation. If the values drop below a defined threshold, the process is reinitialized taking as initialization the last computed deformed Template. However, for problems involving large deformations, numerous regridding steps might be required, which is memory-consuming since one needs to store the last computed deformation field before each reinitialization. Numerically, the resulting deformation field (computed as the composite of intermediate deformations) may not fulfill the topology-preserving conditions, even if the intermediate ones do.

In this paper, we propose a theoretically well-motivated algorithm that falls within the framework of a previous work by the second author ([26]). In this preliminary work, the authors, inspired by [25], design a two-step-algorithm enforcing topology preservation, independently of the registration technique used. The algorithm is thus independent of the selected registration model. It can be applied at intermediate steps of the registration process or at the end.

The first step consists in correcting the gradient vector field of the deformation (that does not comply with the topology preservation criteria) at the discrete level in order to fulfill a set of conditions ensuring topology preservation in the continuous domain after bilinear interpolation (see also [25]). Basically, it consists in balancing the gradient vectors of the displacement field u (related to the deformation field φ by the relation $\varphi = \mathrm{id} + u$) by a parameter α belonging to $]0,1[$. The proposed algorithm provides a unique optimal parameter α at each node of the grid. Once the correction stage is achieved, it remains to reconstruct the deformation field, given its full set of discrete gradient vectors. The problem is phrased as a regularized least-squares problem but as is, one would fail to get the uniqueness of the solution (the solutions would be defined up to a constant). It is thus complemented by a constraint on the mean of the deformation field, thus ensuring uniqueness of the solution. The algorithm is shown to be efficient and has demonstrated its ability to handle large deformations. Also, it has been compared with Christensen et al.'s regridding technique on complex slices of brain data in the case of brain mapping to a disk. In many cases, the proposed algorithm outperforms the regridding technique. Nevertheless, some criticisms can be raised:

- First of all, the computations are carried out on the whole image domain, even though the regions exhibiting overlaps are generally very few and localized on the image domain, which leads to superfluous calculations and strays us from real-time computation requirements. In practice, the deformation components are recomputed over the whole domain, altering somewhat the physics of the problem.
- Besides, the constraint that complements the approximation problem (being about the mean of the deformation) is rather artificial and cannot be physically interpreted. It is global and may not render well the complexity of variations of the deformation components.

We thus propose in this paper to decompose the original reconstruction problem into independent problems of smaller dimensions, yielding a natural parallelization of the computations. We localize the regions exhibiting overlaps, and formulate for each domain a functional minimization problem equipped with interpolation constraints on the boundary, reproducing more accurately the physics of the problem. The algorithm acts locally (the deformation is left unaltered where the topology-preserving criterion is fulfilled) and the obtained result thus remains more consistent with the physics of the problem (due also to the Lagrange interpolation constraints stemming from the unaltered deformation field). One could object that when applied at the end of the process, the obtained deformation field is no longer a solution of the optimization process. This is indeed true, but as previously mentioned, the proposed algorithm acts locally and the minimization problems are constrained with Lagrange interpolation constraints stemming from the unaltered deformation. Besides, the proposed algorithm is applied when the registration process produces a deformation field that is itself mechanically and physically meaningless (a minimization problem in registration can be well-posed with the guarantee of existence of minimizers —for instance in the nonlinear elasticity framework—but may numerically generate overlaps). It thus makes sense to correct the obtained deformation field. At last, the algorithm acts on the magnitude of the displacement vectors, not on their direction.

One could also claim that registration models involving controls on the Jacobian determinant are more relevant than the proposed modelling. We answer first, that for many of those methods, no theoretical result of existence of minimizers is provided (or theoretical results are given but the theoretical model is not the one that is implemented

in practice). It thus means that the numerical scheme, at best, makes the energy decrease to the infimum, but the optimization problem does not necessarily admit a minimizer. Besides, some numerical artifices are often used. For instance, for the fluid registration model by Christensen et al., a detailed algorithm is provided in [28]. In the main loop, the displacement vector field is updated in the following way: $\vec{U}^{(k+1)} = \vec{U}^{(k)} + \delta t^{(k)} \delta \vec{U}^{(k)}$ with $\begin{cases} \delta u_{\max}^{(k)} = ||\delta \vec{U}^{(k)}||_V, \\ \delta t^{(k)} = \min\left(1, \mathrm{tol}_u / \delta u_{\max}^{(k)}\right) \end{cases}$. It means that this procedure has the same effect as the method we propose: the direction of the obtained displacement vector field is preserved while the magnitude can be modified. This strategy of rescaling is further discussed p. 183 of [28] for variational non-parametric registration methods.

From the second author's experience, the implementation of such methods (without heavy numerical artifices) does not guarantee either that the obtained deformation field is topology-preserving and fails to correctly align the shapes when the deformations are too large. That is why we took the side of decoupling the registration process from the topology-preserving question. When applied at intermediate steps of the registration process, the corrected deformation field can be interpreted as a new initial condition of the problem. At last, one could also argue that decomposing the original problem into smaller dimension independent ones may destroy the global coupling. For the reasons stated above, we believe that this decoupling does not affect the result. In particular, the proposed results are qualitatively comparable to those presented in [26], when no decomposition into subproblems is considered.

The novelty of the paper thus rests upon:

- the decomposition of the original problem into independent problems of smaller dimensions, enabling us to significantly reduce the computational time (up to a factor 80 for some critical applications).
- the proof of the existence/uniqueness of the solution of the introduced functional minimization problem on each subdomain,
- a theoretical result of convergence when the size of the data to approximate increases to infinity, ensuring the well-posedness of the problem.
- a result of convergence of the method in the discrete setting.
- a precise depiction of the discretization of the problem: generic finite element, basis functions, properties of the systems to be solved, and in particular a result of nonsingularity of the symmetric indefinite matrix involved in the linear systems.

The remainder of the paper is organized as follows. In Section 2, the first step of the method is recalled. Section 3 is dedicated to the modelling of the reconstruction step. Theoretical results are established such as the result of existence/uniqueness of the solution of the involved minimization problem, the characterization of the solution, a result of convergence as well as the discretization of the problem. Section 4 is devoted to numerical simulations demonstrating the ability of the model to handle large deformations and the interest of having decomposed the problem into independent smaller ones from a computational viewpoint. Let us emphasize that the focus of the paper is on the mathematical presentation and well-posedness of the method. Hence, the computational results are currently still restricted to two dimensions. A comment on the extension of the model to 3D is given at the end of Section 3.

2. Correction of the deformation

The first step consists in applying the same procedure as the one adopted by Le Guyader et al. in [26] (inspired by prior related work [25] but slightly different). For the sake of completeness, we remind the reader about this correction stage.

Let Ω be a connected bounded open subset of $\mathbb{R}^2$ representing the reference configuration, with Lipschitz boundary $\partial\Omega$.

Let $h:\left|\begin{array}{l}\overline{\Omega}\to\mathbb{R}^2\\ (x,y)\mapsto h(x,y)=\big(f(x,y),g(x,y)\big)^T\end{array}\right.$ be the deformation of the reference configuration.

A deformation is a smooth mapping that is orientation-preserving and injective except possibly on $\partial\Omega$. We denote by u the displacement field associated with h, i.e., $h=\mathrm{id}+u$.

The deformation gradient is $\nabla h:\overline{\Omega}\to M_2(\mathbb{R})$ defined by $\nabla h=I_2+\nabla u$ with $M_2(\mathbb{R})$ the set of 2×2 real square matrices.

The correction algorithm is based on the following proposition that provides a set of conditions to be fulfilled in the discrete setting to ensure topology preservation in the continuous domain. More precisely, Proposition 2.1 relates conditions of positivity of some discrete Jacobians to a property of topology-preservation in the continuous domain after bilinear interpolation. This approach seems relevant since we work in practice with digital images: the centers of gravity of the pixels coincide with the nodes of the discrete domain.

PROPOSITION 2.1 (From Karaçali and Davatzikos in [25]).

Let $\mathcal{C}$ be the class of deformation fields $\mathsf{h}=(\mathsf{f},\mathsf{g})$ defined over a discrete rectangle $\Omega=[0,1,\ldots,M]\times[0,1,\ldots,N]\subset\mathbb{N}^2$ for which J_{ff}, J_{fb}, J_{bf}, J_{bb} are positive for all $(x,y)\in\Omega$.

Let $\mathsf{h}=(\mathsf{f},\mathsf{g})$ be a deformation field belonging to $\mathcal{C}$. Then its continuous counterpart determined by the interpolation of h over the domain $\Omega_C=[0,M]\times[0,N]\subset\mathbb{R}^2$ using the interpolant Φ given by $\Phi(x,y)=\Psi(x)\Psi(y)$ with

$$\Psi(t)=\begin{cases}1+t & \text{if } -1\le t<0\\ 1-t & \text{if } 0\le t<1\\ 0 & \text{otherwise}\end{cases}$$

preserves topology, with the backward and forward finite difference schemes f_x^b, f_x^f, f_y^b, f_y^f to approximate the partial derivatives of f (similarly for g) and

$$\left|\begin{array}{l}J_{ff}=\mathsf{f}_x^f(p_1)\mathsf{g}_y^f(p_1)-\mathsf{f}_y^f(p_1)\mathsf{g}_x^f(p_1)\\ J_{bf}=\mathsf{f}_x^b(p_2)\mathsf{g}_y^f(p_2)-\mathsf{f}_y^f(p_2)\mathsf{g}_x^b(p_2)\\ J_{fb}=\mathsf{f}_x^f(p_3)\mathsf{g}_y^b(p_3)-\mathsf{f}_y^b(p_3)\mathsf{g}_x^f(p_3)\\ J_{bb}=\mathsf{f}_x^b(p_4)\mathsf{g}_y^b(p_4)-\mathsf{f}_y^b(p_4)\mathsf{g}_x^b(p_4).\end{array}\right.$$

We recall (similarly for g) that:

$$\left|\begin{array}{l}\mathsf{f}_x^f(x,y)=\mathsf{f}(x+1,y)-\mathsf{f}(x,y)\\ \mathsf{f}_x^b(x,y)=\mathsf{f}(x,y)-\mathsf{f}(x-1,y)\\ \mathsf{f}_y^f(x,y)=\mathsf{f}(x,y+1)-\mathsf{f}(x,y)\\ \mathsf{f}_y^b(x,y)=\mathsf{f}(x,y)-\mathsf{f}(x,y-1).\end{array}\right.$$

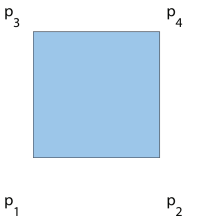

Fig. 2.1: *Layout of the points on a reference square* $[0,1]\times[0,1]$. *This representation is given as an example: only the order of the points* p_1, p_2, p_3 *and* p_4 *matters for the definition of the discrete Jacobians. These points coincide with the centers of gravity of the pixels. In the sequel, these will be denoted by* a_i.

REMARK 2.2. It is shown in [25] that if a deformation field is continuous and globally one-to-one, it preserves topology. It is from this angle that the issue of topology preservation is addressed here. By construction, the continuous counterpart of h denoted by h_c is continuous. The one-to-one property is conditional to the local behavior of h_c: if the continuous deformation field h_c is one-to-one over all square patches that partition the continuous domain defined by the discrete grid, then h_c is globally one-to-one. If we go back to Proposition 2.1, it involves discrete Jacobians, that is, differences. The continuity of the function is thus sufficient to ensure that the mathematical writing is correct. More precisely, inside a given square (for the purpose of illustration $[0,1]\times[0,1]$ and $p_1=(0,0)$, $p_2=(1,0)$, $p_3=(0,1)$ and $p_4=(1,1)$), the components of $\mathsf{h}=(\mathsf{f},\mathsf{g})$ are differentiable (as polynomials) and more precisely, with the notations of Proposition 2.1,

$$\begin{aligned}
\frac{\partial \mathsf{f}}{\partial x}(x,y) &= (\mathsf{f}(1,0)-\mathsf{f}(0,0))(1-y)+(\mathsf{f}(1,1)-\mathsf{f}(0,1))(1-y),\\
\frac{\partial \mathsf{g}}{\partial x}(x,y) &= (\mathsf{g}(1,0)-\mathsf{g}(0,0))(1-y)+(\mathsf{g}(1,1)-\mathsf{g}(0,1))(1-y),\\
\frac{\partial \mathsf{f}}{\partial y}(x,y) &= (\mathsf{f}(1,1)-\mathsf{f}(1,0))x+(\mathsf{f}(0,1)-\mathsf{f}(0,0))(1-x),\\
\frac{\partial \mathsf{g}}{\partial y}(x,y) &= (\mathsf{g}(1,1)-\mathsf{g}(1,0))x+(\mathsf{g}(0,1)-\mathsf{g}(0,0))(1-x),
\end{aligned}$$

and after intermediate computations, the Jacobian determinant $J=J(x,y)$ is given by:

$$J(x,y)=J_{bf}\,x(1-y)+J_{ff}\,(1-x)(1-y)+J_{bb}\,xy+J_{fb}\,(1-x)y,$$

that is, a convex combination of the 4 positive discrete Jacobians. It means that the Jacobian determinant J is positive everywhere inside the square patch. Continuity of the bilinear interpolant provides continuity of h_c over the square and h_c is locally one-to-one over all such squares and globally one-to-one over the domain.

The general idea resulting from Proposition 2.1 is to balance, at the discrete level and at each node of the grid, the gradients of the displacement vectors by a parameter $\alpha\in]0,1[$, in order to comply with the above conditions of positivity of the discrete Jacobians. The construction of the algorithm is motivated by the following observation. In the continuous domain, if we decompose the deformation field $h=(f,g)$ into $h=\mathrm{id}+u$

with $u=(u_1,u_2)$ the displacement vector field, we can compute the Jacobian $J(x,y)$ at any point (x,y).

If now we focus on the related deformation field $h_\alpha:(x,y)\mapsto(\mathrm{id}+\alpha u)(x,y)=(f_\alpha(x,y),g_\alpha(x,y))=(x+\alpha u_1(x,y),y+\alpha u_2(x,y))$, we can similarly calculate the Jacobian $J_\alpha(x,y)$ at any point (x,y) by:

$$J_\alpha(x,y)=\left(1+\alpha\frac{\partial u_1}{\partial x}(x,y)\right)\left(1+\alpha\frac{\partial u_2}{\partial y}(x,y)\right)-\alpha^2\frac{\partial u_2}{\partial x}(x,y)\frac{\partial u_1}{\partial y}(x,y).$$

It exhibits the following properties:

- $J_\alpha(x,y)$ is a polynomial of order 2 in α,
- $\lim_{\alpha\to 0}J_\alpha(x,y)=1$,
- $\lim_{\alpha\to 1}J_\alpha(x,y)=J(x,y)$.

If we suppose that $J(x,y)<0$ then, according to the intermediate value theorem, there exists $\alpha^*\in]0,1[$ such that $J_{\alpha^*}(x,y)=\varepsilon\in[0,1]$. The idea is thus to confine the Jacobian values to a positive interval by correcting the gradients of the displacement vector field.

Strictly, we should consider the deformation field defined by $h_\alpha:(x,y)\mapsto(x+\alpha(x,y)u_1(x,y),y+\alpha(x,y)u_2(x,y))$ in the continuous domain.

But the aim is to adapt the previous idea to the discrete setting. At each node of the grid, a correction parameter is computed and applied not to the displacement vector field itself, but to the gradients of the displacement vector field. Note that applying the correction stage at the level of the displacement vector field itself would not guarantee that the discrete Jacobians obtained fulfill the conditions of Proposition 2.1.

We adapt the previous idea to the discrete setting: the algorithm produces a unique optimal correction parameter α at each node. If $J(x,y)<0$, there are four possible shapes for $J_\alpha(x,y)$:

1. $J_\alpha(x,y)$ reaches its minimum over $]0,1]$ (cf. Figure 2.2, solid line),
2. $J_\alpha(x,y)$ reaches its minimum over $]1,+\infty]$ (cf. Figure 2.2, dotted line),
3. $J_\alpha(x,y)$ reaches its maximum over $[0,1[$ (cf. Figure 2.2, dashed line),
4. $J_\alpha(x,y)$ reaches its maximum over $]-\infty,0]$ (cf. Figure 2.2, dash-dotted line).

Consequently, if $\alpha^*\in]0,1[$ is such that $J_{\alpha^*}(x,y)=0$, then for $0<\alpha<\alpha^*$, $J_\alpha(x,y)>0$. For instance, suppose that for a given node, the four Jacobians are negative (in practice, this is the most common case). Then we compute four correction parameters α^*_{ff}, α^*_{fb}, α^*_{bf} and α^*_{bb} associated to each combination. It suffices to take the minimum of these four values to guarantee that the four Jacobians are positive.

Now suppose that three Jacobians are negative, for instance, J_{ff}, J_{bf} and J_{fb}. Then we compute α^*_{ff}, α^*_{fb} and α^*_{bf}, and we set $\alpha_{int}=\min(\alpha^*_{ff},\alpha^*_{fb},\alpha^*_{bf})$. The second-degree polynomial in α, J^α_{bb} is computed for α_{int}. If $J^{\alpha_{int}}_{bb}(x,y)>0$, then $\alpha^*=\alpha_{int}$, otherwise we take $\alpha^*=\min\left(roots(J^\alpha_{bb}(x,y))\right)$. And so on for the other cases.

The algorithm thus provides a unique optimal correction parameter per grid node (when necessary) and the approximated gradients of the displacement vector field are corrected in compliance with the obtained correction parameters.

Thanks to this parameter α, we can compute the corrected (when necessary) Jacobian matrix at the considered grid node: the output of the first step is then this discrete set of corrected (when necessary) Jacobian matrices hereinafter denoted by $\{\omega_i\}$.

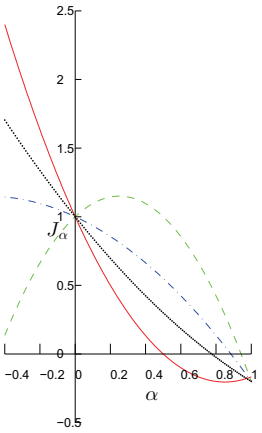

Fig. 2.2: *The four possible representations of the Jacobian.*

3. Deformation reconstruction

The issue to be addressed now lies in the reconstruction of the deformation field, given its discrete set of gradients, with the fewest computations possible (real-time computations should be expected).

Unlike our previous model on this topic, formulated as a functional minimization problem on the whole domain Ω (meaning in particular that the computations were made even on regions of the deformation map complying with the orientation-preserving requirement), we propose to concentrate the computational effort on the subdomains of the deformation grid exhibiting overlaps and to set Lagrange interpolation conditions on the boundary of the subdomains, reproducing more faithfully the physics of the problem. This allows us to apply the reconstruction process on each region independently and to reduce significantly the computational cost. In the sequel, we assume that we have identified (manually for the moment) $\mathcal{N}$ nonempty connected bounded open subsets Ω_i of Ω with Lipschitz boundary, $i \in \{1,\cdots,\mathcal{N}\}$ on which orientation preservation is violated. $\forall i \in \{1,\cdots,\mathcal{N}\}$, $\Omega_i \subset \Omega$ and $\Omega_i \cap \Omega_j = \emptyset$ for $i \neq j$. We then introduce our mathematical model of reconstruction, valid for each subdomain Ω_i, $i \in \{1,\cdots,\mathcal{N}\}$. A D^m-spline approach is retained (cf. [2]). Generally speaking, the D^m-splines over an open subset of $\mathbb{R}^n$ are multidimensional minimizing splines, i.e., functions defined on Ω subjected to interpolation or smoothing conditions and that minimize an energy functional involving derivatives of order m. This choice of methodology is guided by the authors' experience in the field of approximation. This technique proves to be very satisfactory both in terms of theory (convergence results validate the approach) and applications: it provides accurate results. Here again we refer the reader to [2] for more details. Of course, other strategies could have been considered.

3.1. Functional to be minimized. We remind the reader that $\forall i \in \{1,\cdots,\mathcal{N}\}$, Ω_i is a nonempty connected bounded open subset of $\Omega \subset \mathbb{R}^2$ with Lipschitz boundary. Let ν be an integer such that $\nu \in \{1,\cdots,\mathcal{N}\}$. Inspired by the D^m-spline approach, we introduce a regularized least-squares problem defined on a space of vector-valued functions, in order to fit the discrete set of corrected gradient vectors of the defor-

mation and to satisfy Lagrange interpolation constraints. More precisely, the problem is phrased as a constrained functional minimization problem on a convex subspace of the Hilbert space $\mathrm{H}^3(\Omega_\nu,\mathbb{R}^2)$ so that the Sobolev's embedding $\mathrm{H}^3(\Omega_\nu,\mathbb{R}^2)\circlearrowleft\mathrm{C}^1(\overline{\Omega_\nu},\mathbb{R}^2)$ holds (it means that the inclusion of $\mathrm{H}^3(\Omega_\nu,\mathbb{R}^2)$ into $\mathrm{C}^1(\overline{\Omega_\nu},\mathbb{R}^2)$ is continuous, that is to say: $\mathrm{H}^3(\Omega_\nu,\mathbb{R}^2)\subset\mathrm{C}^1(\overline{\Omega_\nu},\mathbb{R}^2)$ and there exists $C>0$, depending only on Ω_ν, such that $\forall u\in\mathrm{H}^3(\Omega_\nu,\mathbb{R}^2), \|u\|_{\mathrm{C}^1(\overline{\Omega_\nu},\mathbb{R}^2)}\leq C\|u\|_{\mathrm{H}^3(\Omega_\nu,\mathbb{R}^2)}$, see [1] or [8]). It guarantees, in particular, that the pointwise fitting term dealing with the derivatives of the unknown is well-defined. We thus rebuild a smoother-than-required deformation field (by smoother, we mean more regular) but retain only the values of the deformation components obtained at the grid nodes (centers of gravity of the pixels). Before depicting our model, we introduce some fundamental mathematical notions that will be useful to state the functional minimization problem.

For any $\gamma=(\gamma_1,\gamma_2)\in\mathbb{N}^2$, we write $|\gamma|=\gamma_1+\gamma_2$ and $\partial^\gamma=\dfrac{\partial^{|\gamma|}}{\partial x_1^{\gamma_1}\partial x_2^{\gamma_2}}$. We recall the standard inner product and the induced norm on $\mathrm{H}^3(\Omega_\nu,\mathbb{R}^2)$:

$$((u,v))_{\mathrm{H}^3(\Omega_\nu,\mathbb{R}^2)}=\sum_{|\gamma|\leq 3}\int_{\Omega_\nu}\langle\partial^\gamma u,\partial^\gamma v\rangle_2\,\mathrm{d}x_1\,\mathrm{d}x_2 \text{ and } \|v\|^2_{\mathrm{H}^3(\Omega_\nu,\mathbb{R}^2)}=((v,v))_{\mathrm{H}^3(\Omega_\nu,\mathbb{R}^2)},$$

and the semi-inner product and the semi-norm:

$$(u,v)_{3,\Omega_\nu,\mathbb{R}^2}=\sum_{|\gamma|=3}\int_{\Omega_\nu}\langle\partial^\gamma u,\partial^\gamma v\rangle_2\,\mathrm{d}x_1\,\mathrm{d}x_2 \text{ and } |v|^2_{3,\Omega_\nu,\mathbb{R}^2}=(v,v)_{3,\Omega_\nu,\mathbb{R}^2}$$

where $\langle\cdot,\cdot\rangle_2$ denotes the Euclidean scalar product in $\mathbb{R}^2$. For the sake of clarity, we recall the general definition of a P-unisolvent set.

Definition 3.1 (see [2]). *For any $l\in\mathbb{N}$, we denote by P_l the space of polynomial functions defined over $\mathbb{R}^n$ of degree $\leq l$ with respect to the set of variables, and for any $l\in\mathbb{N}$ and for any nonempty connected open subset Ω in $\mathbb{R}^n$, by $P_l(\Omega)$ the space of restrictions to Ω of the functions in P_l. A set $A=\{a_1,\cdots,a_N\}$ of N points of $\mathbb{R}^n$ is P_l-unisolvent if $\forall\{\alpha_1,\cdots,\alpha_N\}\subset\mathbb{R}$, $\exists!\Psi\in P_l$, $\forall i\in\{1,\cdots,N\}$, $\Psi(a_i)=\alpha_i$.*

In particular, $\exists!\Psi\in P_l$, $\forall i\in\{1,\cdots,N\}$, $\Psi(a_i)=0$. It is clear that a necessary condition for the set A to be P_l-unisolvent is that $N=dimP_l$.

Let $A=\{a_i\}_{i=1,\cdots,N}$ be a set of N points of $\overline{\Omega_\nu}$ containing a P_1-unisolvent subset. As the set A contains a P_1-unisolvent subset, we can only infer that $N\geq\dim\ P_1$. In our application, the set A is made of the coordinates of the image pixels included in $\overline{\Omega_\nu}$.

Let also $\{\omega_i\}_{i=1,\cdots,N}$ be the set of N Jacobian matrices of the deformation given at $\{a_i\}_{i=1,\cdots,N}$. This set is made of the corrected gradient vectors of the deformation obtained at the correction step of the algorithm. At last, let $\{b_i\}_{i=1,\cdots,l}$ be l points of $\overline{\Omega_\nu}$ where the discrete gradient vectors of the deformation have been unaltered (so the deformation is unchanged). In all our applications, these points will belong to the boundary $\partial\Omega_\nu$ of Ω_ν. We set Lagrange interpolation constraints at these points (see Figure 3.1). It means that if h denotes the unaltered deformation and v denotes the unknown deformation of the minimization problem, we must have:

$$\forall i\in\{1,\cdots,l\},\ v(b_i)=h(b_i).$$

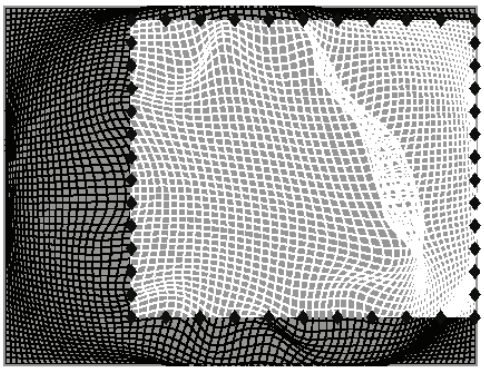

Fig. 3.1: *Example of a subdomain (white zone) $\Omega_1 \subset \Omega$ on the boundary of which, interpolation conditions are prescribed (black dots representing the b_i, $i \in \{1,\cdots,l\}$).*

Let K be the set defined by $K = \{v \in \mathrm{H}^3(\Omega_\nu,\mathbb{R}^2), \beta(v) = \eta\}$, with β the mapping:

$$\beta : \left| \begin{array}{l} \mathrm{H}^3(\Omega_\nu,\mathbb{R}^2) \to \mathbb{R}^{2l} \\ v \mapsto \beta(v) = \big(v(b_1),\cdots,v(b_l)\big)^T \end{array} \right.$$

and $\eta = \big(h(b_1),\cdots,h(b_l)\big)^T$. The convex set K is closed as the reciprocal image of a closed set by a continuous mapping (see [8]). The approximation problem can be stated as follows: given the set of N Jacobian matrices defined at $\{a_i\}_{i=1,\cdots,N}$, search for v sufficiently smooth such that $\forall i \in \{1,\cdots,N\}$, the Jacobian matrix Dv evaluated at a_i is close to w_i and such that $\forall i \in \{1,\cdots,l\}$, $v(b_i) = h(b_i)$. For this purpose, we need the following additional notations. We denote by ρ the operator defined by:

$$\rho : \left| \begin{array}{l} H^2(\Omega_\nu,\mathbb{R}^{2\times 2}) \to (\mathbb{R}^{2\times 2})^N \\ v \mapsto \rho(v) = \big(v(a_1), v(a_2),\cdots,v(a_N)\big)^T \end{array} \right. . \tag{3.1}$$

The problem is then cast as an optimization one by means of the functional $\mathcal{J}_\epsilon$ defined by:

$$\mathcal{J}_\epsilon : \left| \begin{array}{l} \mathrm{H}^3(\Omega_\nu,\mathbb{R}^2) \to \mathbb{R} \\ v \mapsto \langle \rho(Dv) - w \rangle_N^2 + \epsilon |v|^2_{3,\Omega_\nu,\mathbb{R}^2}, \end{array} \right.$$

with $\epsilon > 0$ a tuning parameter and with $w = \big(w_1, w_2,\cdots,w_N\big)^T \in \big(\mathbb{R}^{2\times 2}\big)^N$. The operator $\langle\cdot,\cdot\rangle_N$ is defined as follows: $\forall \xi \in \big(\mathbb{R}^{2\times 2}\big)^N, \forall \eta \in \big(\mathbb{R}^{2\times 2}\big)^N$, $\langle \xi,\eta\rangle_N = \displaystyle\sum_{i=1}^{N}\sum_{j=1}^{4} \xi_{ij}\eta_{ij}$ and $\langle\xi\rangle_N = \langle \xi,\xi\rangle_N^{\frac{1}{2}}$. The first term of the functional $\mathcal{J}_\epsilon$ ensures closeness to the data while the second component is a regularizing component. We consider the following minimization problem:

$$\left\{ \begin{array}{l} \text{Search for } \sigma_\epsilon \in K \text{ such that} \\ \forall v \in K,\ \mathcal{J}_\epsilon(\sigma_\epsilon) \le \mathcal{J}_\epsilon(v). \end{array} \right. \tag{3.2}$$

We can notice that minimizing $\mathcal{J}_\epsilon$ with respect to v is equivalent to minimizing:

$$\langle \rho(Dv)\rangle_N^2 - 2\langle \rho(Dv),\omega\rangle_N + \epsilon |v|^2_{3,\Omega_\nu,\mathbb{R}^2}.$$

From now on, we thus denote by $\mathcal{J}_\epsilon$ the new functional:

$$\mathcal{J}_\epsilon : \left| \begin{array}{l} \mathrm{H}^3(\Omega_\nu,\mathbb{R}^2) \to \mathbb{R} \\ v \mapsto \langle \rho(Dv)\rangle_N^2 - 2\langle \rho(Dv),\omega\rangle_N + \epsilon |v|^2_{3,\Omega_\nu,\mathbb{R}^2}. \end{array} \right.$$

Our goal being to prove the existence/uniqueness of the solution of the introduced functional minimization problem, we rephrase functional $\mathcal{J}_\epsilon$ in terms of the bilinear form a and the linear form L defined hereafter. Let a be the symmetric bilinear form such that:

$$\mathsf{a} : \left| \begin{array}{l} \mathrm{H}^3(\Omega_\nu,\mathbb{R}^2) \times \mathrm{H}^3(\Omega_\nu,\mathbb{R}^2) \to \mathbb{R} \\ (u,v) \mapsto \langle \rho(Du), \rho(Dv)\rangle_N + \epsilon (u,v)_{3,\Omega_\nu,\mathbb{R}^2}. \end{array} \right.$$

Let also L be the linear form defined by:

$$L : \left| \begin{array}{l} \mathrm{H}^3(\Omega_\nu,\mathbb{R}^2) \to \mathbb{R} \\ v \mapsto \langle \rho(Dv),\omega\rangle_N \end{array} \right. .$$

The minimization problem thus becomes:

$$\begin{cases} \text{Search for } \sigma_\epsilon \in K \text{ such that} \\ \forall v \in K, \mathsf{a}(\sigma_\epsilon,\sigma_\epsilon) - 2L(\sigma_\epsilon) \le \mathsf{a}(v,v) - 2L(v). \end{cases} \tag{3.3}$$

The mappings a and L are continuous, but the trouble is that the bilinear form a is not $\mathrm{H}^3(\Omega_\nu,\mathbb{R}^2)$-elliptic, which prevents us from applying Stampacchia's theorem ([8]) straightforwardly. To circumvent this issue, we introduce an artificial term in the minimization problem formulation as follows:

$$\begin{cases} \text{Search for } \sigma_\epsilon \in K \text{ such that} \\ \forall v \in K, \mathsf{a}(\sigma_\epsilon,\sigma_\epsilon) - 2L(\sigma_\epsilon) + \|\beta(\sigma_\epsilon)\|^2_{2l} \le \mathsf{a}(v,v) - 2L(v) + \|\beta(v)\|^2_{2l}. \end{cases} \tag{3.4}$$

This new phrasing involves the bilinear form denoted by $\hat{a}$ defined by

$$\hat{\mathsf{a}} : \left| \begin{array}{l} \mathrm{H}^3(\Omega_\nu,\mathbb{R}^2) \times \mathrm{H}^3(\Omega_\nu,\mathbb{R}^2) \to \mathbb{R} \\ (u,v) \mapsto \mathsf{a}(u,v) + \langle \beta(u),\beta(v)\rangle_{2l} \end{array} \right.$$

and the following propositions hold.

PROPOSITION 3.2. *The mapping* $\|\widehat{\cdot}\|$ *defined on* $\mathrm{H}^3(\Omega_\nu,\mathbb{R}^2)$ *by*

$$\|\widehat{\cdot}\| : \left| \begin{array}{l} \mathrm{H}^3(\Omega_\nu,\mathbb{R}^2) \to \mathbb{R} \\ v \mapsto \sqrt{\hat{\mathsf{a}}(v,v)} \end{array} \right.$$

is an Hilbertian norm.

Proof. The proof is based on the argument of connectedness of Ω_ν and the property of P_1-unisolvence of the set A.

- It is obvious that $\|\widehat{\lambda v}\| = |\lambda| \|\widehat{v}\|$, $\forall \lambda \in \mathbb{R}$ according to the definition of $\hat{\mathsf{a}}$.

- The triangle inequality is also obvious as a result of the definition of $\hat{\mathsf{a}}$ and the inner product.
- Let us prove that $\|\widehat{v}\| = 0 \Rightarrow v \equiv 0$.
  Let $v \in \mathrm{H}^3(\Omega_\nu, \mathbb{R}^2)$ be such that $\|\widehat{v}\| = 0$.
  It implies that:
  - $|v|_{3,\Omega_\nu,\mathbb{R}^2} = 0$ and as Ω_ν is connected, it yields $v \in P_2(\Omega_\nu, \mathbb{R}^2)$.
  - Also, $<\rho(Dv)>_N = 0$. As $v \in P_2(\Omega_\nu, \mathbb{R}^2)$, it follows that $Dv \in P_1(\Omega_\nu, \mathbb{R}^{2\times 2})$ and from the unisolvence property we conclude that $Dv = 0_{\mathbb{R}^{2\times 2}}$. The mapping v can thus be written as $v = \begin{pmatrix} c_1 \\ c_2 \end{pmatrix}$ where c_1 and c_2 are constants.
  - At last, $<\beta(v)>^2_{\mathbb{R}^{2l}} = 0 \Leftrightarrow \beta(v) = 0_{\mathbb{R}^{2l}}$ and so $c_1 = c_2 = 0$.

  It yields $v \equiv 0$.

□

PROPOSITION 3.3. *The norm $\|\widehat{.}\|$ is equivalent to the norm $\|.\|_{\mathrm{H}^3(\Omega_\nu,\mathbb{R}^2)}$ on $\mathrm{H}^3(\Omega_\nu, \mathbb{R}^2)$.*

Proof. The proof is based on a theorem of equivalence of norms by Nečas (Theorem 7.1, [31]) and on the continuity of the bilinear form $\widehat{\mathsf{a}}$ on $\mathrm{H}^3(\Omega_\nu,\mathbb{R}^2) \times \mathrm{H}^3(\Omega_\nu,\mathbb{R}^2)$.
The continuity of the bilinear form $\widehat{\mathsf{a}}$ results from the continuity of a and the following inequality: $\forall (u,v) \in \mathrm{H}^3(\Omega_\nu,\mathbb{R}^2) \times \mathrm{H}^3(\Omega_\nu,\mathbb{R}^2)$,
$|<\beta(u),\beta(v)>_{\mathbb{R}^{2l}}| \leq |\beta(u)|_{\mathbb{R}^{2l}} |\beta(v)|_{\mathbb{R}^{2l}}$ (Cauchy–Schwarz inequality)
with $|\beta(u)|_{\mathbb{R}^{2l}} = \sqrt{\sum_{i=1}^{l} <u(b_i)>_2^2}$.
But $<u(b_i)>_2 \leq \|u\|_{\mathrm{C}^0(\overline{\Omega_\nu},\mathbb{R}^2)}$ with $\|u\|_{\mathrm{C}^0(\overline{\Omega_\nu},\mathbb{R}^2)} = \sup_{x\in\overline{\Omega_\nu}} <u(x)>_2$ and using the Sobolev's embedding theorem, we have : $<u(b_i)>_2 \leq C\|u\|_{\mathrm{H}^3(\Omega_\nu,\mathbb{R}^2)}$.
Therefore, $|\beta(u)|_{\mathbb{R}^{2l}} \leq \sqrt{l} C \|u\|_{\mathrm{H}^3(\Omega_\nu,\mathbb{R}^2)}$ and

$$|<\beta(u),\beta(v)>_{\mathbb{R}^{2l}}| \leq lC^2 \|u\|_{\mathrm{H}^3(\Omega_\nu,\mathbb{R}^2)} \|v\|_{\mathrm{H}^3(\Omega_\nu,\mathbb{R}^2)}.$$

The bilinear form $\widehat{\mathsf{a}}$ being continuous on $\mathrm{H}^3(\Omega_\nu,\mathbb{R}^2) \times \mathrm{H}^3(\Omega_\nu,\mathbb{R}^2)$, there exists a constant $c > 0$ such that $\forall v \in \mathrm{H}^3(\Omega_\nu,\mathbb{R}^2)$:

$$\widehat{\mathsf{a}}(v,v) = \|\widehat{v}\|^2 \leq c\|v\|^2_{\mathrm{H}^3(\Omega_\nu,\mathbb{R}^2)}.$$

For the second part of the inequality, we use Nečas' theorem with $k=3$ and $p=2$. We take $\frac{1}{\sqrt{\epsilon}}\rho$ for f_1 and $\frac{1}{\sqrt{\epsilon}}\beta$ for f_2. $\forall v \in P_2(\Omega_\nu,\mathbb{R}^2)$, $\sum_{i=1}^{2} |f_i v|^2 = 0 \Leftrightarrow v \equiv 0$ from the unisolvence property of the set A. From Nečas' theorem, we then get that there exists a constant $c_1 > 0$ such that:

$$c_1^2 \|v\|^2_{\mathrm{H}^3(\Omega_\nu,\mathbb{R}^2)} \leq |v|^2_{3,\Omega_\nu,\mathbb{R}^2} + \tfrac{1}{\epsilon} <\rho(Dv)>_N^2 + \tfrac{1}{\epsilon}\|\beta(v)\|^2_{\mathbb{R}^{2l}}$$

$$\Leftrightarrow \epsilon c_1^2 \|v\|^2_{\mathrm{H}^3(\Omega_\nu,\mathbb{R}^2)} \leq \epsilon |v|^2_{3,\Omega_\nu,\mathbb{R}^2} + <\rho(Dv)>_N^2 + \|\beta(v)\|^2_{\mathbb{R}^{2l}}$$

$$\Leftrightarrow \|v\|^2_{H^3(\Omega_\nu,\mathbb{R}^2)} \leq \tfrac{1}{\epsilon c_1^2}\|\widehat{v}\|^2.$$ □

It results in the following theorem:

THEOREM 3.4. *Problem (3.2) admits a unique solution $\sigma_\epsilon \in K$. This solution is characterized by the variational inequality: $\forall v \in K$, $\widehat{\mathsf{a}}(\sigma_\epsilon, v - \sigma_\epsilon) \geq L(v - \sigma_\epsilon)$.*

Proof. The proof is based on Stampacchia's theorem ([8]). □

3.2. Characterization of the solution. Let K_0 be the vector subspace of $\mathrm{H}^3(\Omega_\nu,\mathbb{R}^2)$ defined by

$$K_0=\{v\in \mathrm{H}^3(\Omega_\nu,\mathbb{R}^2)\mid \beta(v)=0_{\mathbb{R}^{2l}}\}.$$

Let S be the set defined by

$$S=\{u\in \mathrm{H}^3(\Omega_\nu,\mathbb{R}^2)\mid \forall v\in K_0, \mathsf{a}(u,v)=L(v)\}.$$

Then the following proposition holds:

PROPOSITION 3.5. *The unique solution σ_ϵ of problem (3.2) is characterized by:*

$$\{\sigma_\epsilon\}=K\cap S.$$

This is mainly an abstract result that will be useful to prove Theorem 3.6.

Proof. First, let us prove that $\{\sigma_\epsilon\}\subset K\cap S$.
From Stampacchia's theorem, we have $\forall v\in K$:

$$\widehat{\mathsf{a}}(\sigma_\epsilon,v-\sigma_\epsilon)\geq L(v-\sigma_\epsilon).$$

But $v-\sigma_\epsilon\in K_0$ so $\widehat{\mathsf{a}}(\sigma_\epsilon,v-\sigma_\epsilon)=\mathsf{a}(\sigma_\epsilon,v-\sigma_\epsilon)\geq L(v-\sigma_\epsilon)$.
Moreover, $-(v-\sigma_\epsilon)\in K_0$ since K_0 is a vector space, so $\forall v\in K$:

$$\widehat{\mathsf{a}}(\sigma_\epsilon,-(v-\sigma_\epsilon))\geq L(-(v-\sigma_\epsilon))\Longleftrightarrow \widehat{\mathsf{a}}(\sigma_\epsilon,v-\sigma_\epsilon)\leq L(v-\sigma_\epsilon).$$

By gathering the two above results, it yields $\widehat{\mathsf{a}}(\sigma_\epsilon,v-\sigma_\epsilon)=L(v-\sigma_\epsilon)$, which means that $\forall v_0\in K_0, \mathsf{a}(\sigma_\epsilon,v_0)=L(v_0)$.

Therefore $\sigma_\epsilon\in K\cap S$. Now, let us prove that $K\cap S\subset\{\sigma_\epsilon\}$. Let $w\in K\cap S$. So $w\in K$ and $\forall v_0\in K_0, \mathsf{a}(w,v_0)=L(v_0).\forall v\in K, v-w\in K_0$ so:

$$\mathsf{a}(w,v-w)=L(v-w)\geq L(v-w).$$

Therefore, w is a solution of Problem (3.2) and by uniqueness of the solution, $w=\sigma_\epsilon$. It yields $K\cap S\subset\{\sigma_\epsilon\}$. ∎

3.3. Lagrange multipliers. We now introduce Lagrange multipliers, which enables us to define the variational formulation of problem (3.2) on the whole space $\mathrm{H}^3(\Omega_\nu,\mathbb{R}^2)$ and to obtain a variational equality (efficiently tractable in the context of the Finite Element Method) instead of a variational inequality. Let $K_0^\perp$ be the orthogonal complement of K_0 in $\mathrm{H}^3(\Omega_\nu,\mathbb{R}^2)$ for the scalar product $\widehat{\mathsf{a}}(\cdot,\cdot)$:

$$K_0^\perp=\{u\in \mathrm{H}^3(\Omega_\nu,\mathbb{R}^2)\mid \widehat{\mathsf{a}}(u,v)=0, \forall v\in K_0\}.$$

The space $\mathrm{H}^3(\Omega_\nu,\mathbb{R}^2)$ can be written as the direct sum $\mathrm{H}^3(\Omega_\nu,\mathbb{R}^2)=K_0^\perp\oplus K_0$. Let us denote by $\beta_{|K_0^\perp}$ the restriction of β to $K_0^\perp$. Then $\beta_{|K_0^\perp}$ is a topological isomorphism (in particular, it is obvious that $\ker\beta_{|K_0^\perp}=K_0\cap K_0^\perp=\{0\}$). The main theorem is stated as follows:

THEOREM 3.6. *If σ_ϵ is the unique solution of problem (3.2), then σ_ϵ is also the solution of the following problem with Lagrange multipliers:*

$$\begin{cases}\text{Search for } (\sigma_\epsilon,\lambda)\in K\times\mathbb{R}^{2l},\\ \forall v\in \mathrm{H}^3(\Omega_\nu,\mathbb{R}^2), \mathsf{a}(\sigma_\epsilon,v)-L(v)+\langle\lambda,\beta(v)\rangle_{2l}=0.\end{cases}\tag{3.5}$$

Proof. Assume that $(u,\lambda)\in K\times\mathbb{R}^{2l}$ is a solution of problem (3.5). Then $\forall v\in K_0$, we have:

$$\mathsf{a}(u,v)-L(v)=0,$$

since $\beta(v)=0_{\mathbb{R}^{2l}}$. Thus $u\in K\cap S$ and from Proposition 3.5, $u=\sigma_\epsilon$.
Conversely, from Proposition 3.5, $\{\sigma_\epsilon\}=K\cap S$ so $\forall v_0\in K_0, \mathsf{a}(\sigma_\epsilon,v_0)=L(v_0)$. Let us consider the linear form defined $\forall w\in K_0^\perp$ by:

$$\mathcal{L}:\left|\begin{array}{l}K_0^\perp\to\mathbb{R}\\ w\mapsto-\mathsf{a}(\sigma_\epsilon,w)+L(w).\end{array}\right.$$

We remind the reader that, denoting by E and F two normed vector spaces and by A a continuous linear mapping from E to F, the adjoint operator $A^t:F'\to E'$ is defined by:

$$\forall v\in E,\forall w\in F', <A^tw,v>_{E',E}=<w,Av>_{F',F}.$$

The mapping $\beta_{|K_0^\perp}:K_0^\perp\to\mathbb{R}^{2l}$ is a topological isomorphism and consequently so is the mapping $\beta^t_{|K_0^\perp}:\mathbb{R}^{2l}\to(K_0^\perp)'$.

As $\mathcal{L}\in(K_0^\perp)'$, there exists a unique $\lambda\in\mathbb{R}^{2l}$ such that $\beta^t_{|K_0^\perp}(\lambda)=\mathcal{L}$. It means that:

$$\begin{aligned}\mathcal{L}(w)=-\mathsf{a}(\sigma_\epsilon,w)+L(w)&=<\beta^t_{|K_0^\perp}(\lambda),w>_{(K_0^\perp)',K_0^\perp},\\ &\Longleftrightarrow \mathsf{a}(\sigma_\epsilon,w)-L(w)+<\beta^t_{|K_0^\perp}(\lambda),w>_{(K_0^\perp)',K_0^\perp}=0,\\ &\Longleftrightarrow \mathsf{a}(\sigma_\epsilon,w)-L(w)+<\lambda,\beta_{|K_0^\perp}(w)>_{(\mathbb{R}^{2l})',\mathbb{R}^{2l}}=0.\end{aligned}$$

Let $v\in\mathrm{H}^3(\Omega_\nu,\mathbb{R}^2)$. Since $\mathrm{H}^3(\Omega_\nu,\mathbb{R}^2)=K_0^\perp\oplus K_0$, $\exists!(v_0,w)\in K_0^\perp\times K_0, v=v_0+w$.
From the last equality, it yields $\exists!\lambda\in\mathbb{R}^{2l}$, such that $\forall v\in\mathrm{H}^3(\Omega_\nu,\mathbb{R}^2)$:

$$\begin{aligned}&\mathsf{a}(\sigma_\epsilon,v)-L(v)-\mathsf{a}(\sigma_\epsilon,v_0)+L(v_0)+<\lambda,\beta(w)>_{(\mathbb{R}^{2l})',\mathbb{R}^{2l}}=0,\\ \Longleftrightarrow&\mathsf{a}(\sigma_\epsilon,v)-L(v)+<\lambda,\beta(w)>_{(\mathbb{R}^{2l})',\mathbb{R}^{2l}}=0,\end{aligned}$$

since $v_0\in K_0$, and $\mathsf{a}(\sigma_\epsilon,v_0)=L(v_0)$ from Proposition 3.5. To conclude, $\beta(w)=\beta(v-v_0)=\beta(v)$ since $\beta(v_0)=0_{\mathbb{R}^{2l}}$.

Finally,

$$\exists!\lambda\in\mathbb{R}^{2l},\forall v\in\mathrm{H}^3(\Omega_\nu,\mathbb{R}^2),\mathsf{a}(\sigma_\epsilon,v)-L(v)+<\lambda,\beta(v)>_{(\mathbb{R}^{2l})',\mathbb{R}^{2l}}=0$$

□

3.4. Theoretical convergence result. We now provide a theoretical convergence result that is an abtract result highlighting the well-posedness of the modelling. Let D be a subset of $]0,+\infty[$ admitting 0 as an accumulation point (this implies that $0\in\overline{D}$). For each $d\in D$, let A^d be a set of $N=N(d)$ distinct points of $\overline{\Omega_\nu}$ containing a P_1-unisolvent subset (we cannot say much on N except that $N\geq\dim P_1$ and as d tends to 0, $N(d)$ increases to $+\infty$).

We suppose that

$$\sup_{x\in\Omega_\nu}\delta(x,A^d)=d, \tag{3.6}$$

where δ is the Euclidean distance in $\mathbb{R}^2$. Let us observe that the left-hand side of (3.6) is just the Hausdorff distance between A^d and $\overline{\Omega_\nu}$. Consequently, it implies that D is bounded and that this distance tends to 0 as d does. Thus d is the radius of the largest sphere included in Ω_ν that contains no point from A^d (Hausdorff distance). Let us remark the ambiguity in the meaning of d defined first as an index and next, independently, in (3.6). This situation is analogous to that found in the Finite Element theory (see [2] and [12]).

We point out that the hypotheses $0 \in \overline{D}$ and (3.6) imply the weaker condition

$$\lim_{d\to 0} \sup_{x\in\Omega_\nu} \delta(x, A^d) = 0. \tag{3.7}$$

For all $d \in D$, we denote by ρ^d the mapping defined by:

$$\rho^d : \left| \begin{array}{l} H^2(\Omega_\nu, \mathbb{R}^{2\times 2}) \to (\mathbb{R}^{2\times 2})^{N(d)} \\ v \mapsto \rho^d(v) = \big((v(a))_{a\in A^d}\big)^T \end{array} \right. .$$

Then we introduce the norm $\|\widehat{\cdot}\|_d$ equivalent to the norm $\|\cdot\|_{\mathrm{H}^3(\Omega_\nu,\mathbb{R}^2)}$ on $\mathrm{H}^3(\Omega_\nu, \mathbb{R}^2)$ defined by: $\forall v \in \mathrm{H}^3(\Omega_\nu, \mathbb{R}^2)$,

$$\|\widehat{v}\|_d = \big[< \rho^d(Dv) >^2_{N(d)} + \epsilon |v|^2_{3,\Omega_\nu,\mathbb{R}^2} + \|\beta(v)\|^2_{2l} \big]^{\frac{1}{2}}.$$

(It is possible to check that $\|\widehat{\cdot}\|_d$ is a norm by applying similar arguments to those in Proposition 3.2). The following lemma holds and allows to state Theorem 3.8.

LEMMA 3.7. *Suppose that* (3.7) *holds. Let* $A_0 = \{b_{01}, \ldots, b_{0\aleph}\}$ *be a fixed* P_1*-unisolvent subset of* $\overline{\Omega_\nu}$.

$$\forall j = 1, \ldots, \aleph, \quad \exists \big(a^d_{0j}\big)_{d\in D}, \big(\forall d \in D, a^d_{0j} \in A^d\big) \text{ and } \big(b_{0j} = \lim_{d\to 0} a^d_{0j}\big). \tag{3.8}$$

For all $d \in D$, *let* A^d_0 *be the set* $\{a^d_{01}, \ldots, a^d_{0\aleph}\}$ *and* $\|.\|_{A^d_0}$ *be the mapping defined by:* $\forall v \in \mathrm{H}^3(\Omega_\nu, \mathbb{R}^2)$,

$$\|v\|_{A^d_0} = \left[\sum_{j=1}^{\aleph} < Dv(a^d_{0j}) >^2_4 + \epsilon |v|^2_{3,\Omega_\nu,\mathbb{R}^2} + \|\beta(v)\|^2_{2l} \right]^{\frac{1}{2}}.$$

Then, there exists $\mu > 0$ *such that for all* $d \le \mu$, *the set* A^d_0 *is* P_1*-unisolvent and* $\|\widehat{\cdot}\|_{A^d_0}$ *is a norm on* $\mathrm{H}^3(\Omega_\nu, \mathbb{R}^2)$ *uniformly equivalent on* $D \cap]0, \mu]$ *to the norm* $\|\cdot\|_{\mathrm{H}^3(\Omega_\nu,\mathbb{R}^2)}$.

THEOREM 3.8. *Suppose that there exists a function* $\widehat{f} \in K$ *such that for all* $d \in D$: $\rho^d(D\widehat{f}) = \omega$, *and* $\epsilon = \epsilon(d) \in]0, \epsilon_0], \epsilon_0 > 0$.

For all $d \in D$, *we denote by* σ^d_ϵ *the unique solution of problem* (3.2), *then under the above assumptions we have:*

$$\lim_{d\to 0} \|\sigma^d_\epsilon - \widehat{f}\|_{\mathrm{H}^3(\Omega_\nu,\mathbb{R}^2)} = 0.$$

Proof. The proof is divided into four steps.

First step

We start by proving that the sequence $\left(\sigma_\epsilon^d\right)_{\substack{d\in D\cap]0,\mu]\\ \epsilon\in]0,\epsilon_0]}}$ is bounded in $\mathrm{H}^3(\Omega_\nu,\mathbb{R}^2)$ independently of d. By taking $v=\widehat{f}$ in problem (3.2) and using the equivalence of norm given in Lemma 3.7, we establish that:

$$\exists\tilde{\nu}>0,\forall d\in D,\forall\epsilon\in]0,\epsilon_0],\left(d\leq\mu\Rightarrow\|\sigma_\epsilon^d\|_{\mathrm{H}^3(\Omega_\nu,\mathbb{R}^2)}\leq\tilde{\nu}\right).$$

The sequence $\left(\sigma_\epsilon^d\right)_{\substack{d\in D\cap]0,\mu]\\ \epsilon\in]0,\epsilon_0]}}$ is bounded in $\mathrm{H}^3(\Omega_\nu,\mathbb{R}^2)$, so one can extract a subsequence $\left(\sigma_{\epsilon_l}^{d_l}\right)_{l\in\mathbb{N}}$ with $\lim\limits_{l\to\infty}d_l=0$ (since 0 is an accumulation point of D) and $\epsilon_l\in]0,\epsilon_0]$, $\forall l\in\mathbb{N}$ —we assume that $\epsilon=\epsilon(d)$ —that weakly converges to an element of $\mathrm{H}^3(\Omega_\nu,\mathbb{R}^2)$ denoted by f^*.

Second step

In this step, we argue by contradiction and prove that $Df^*=D\widehat{f}$ using compactness arguments (Sobolev's embeddings in Hölder's spaces and Rellich–Kondrachov's theorem, see [8]). Finally, the Lagrange interpolation constraints give us that $f^*=\widehat{f}$.

Third step

The aim is to prove that $\left(\sigma_{\epsilon_l}^{d_l}\right)_{l\in\mathbb{N}}$ strongly converges to $\widehat{f}$ in $\mathrm{H}^3(\Omega_\nu,\mathbb{R}^2)$.
Thanks to Rellich–Kondrachov's compact embedding theorem, we obtain that $\left(\sigma_{\epsilon_l}^{d_l}\right)_{l\in\mathbb{N}}$ strongly converges to $\widehat{f}$ in $\mathrm{H}^2(\Omega_\nu,\mathbb{R}^2)$. Since

$$\|\sigma_{\epsilon_l}^{d_l}-\widehat{f}\|^2_{\mathrm{H}^3(\Omega_\nu,\mathbb{R}^2)}=\|\sigma_{\epsilon_l}^{d_l}-\widehat{f}\|^2_{\mathrm{H}^2(\Omega_\nu,\mathbb{R}^2)}+|\sigma_{\epsilon_l}^{d_l}-\widehat{f}|^2_{3,\Omega_\nu,\mathbb{R}^2},$$

we just need to prove that $\lim\limits_{l\to\infty}|\sigma_{\epsilon_l}^{d_l}-\widehat{f}|_{3,\Omega_\nu,\mathbb{R}^2}=0$.We have:

$$|\sigma_{\epsilon_l}^{d_l}-\widehat{f}|^2_{3,\Omega_\nu,\mathbb{R}^2}=|\sigma_{\epsilon_l}^{d_l}|^2_{3,\Omega_\nu,\mathbb{R}^2}+|\widehat{f}|^2_{3,\Omega_\nu,\mathbb{R}^2}-2(\sigma_{\epsilon_l}^{d_l},\widehat{f})_{3,\Omega_\nu,\mathbb{R}^2}.$$

But $|\sigma_{\epsilon_l}^{d_l}|_{3,\Omega_\nu,\mathbb{R}^2}\leq|\widehat{f}|_{3,\Omega_\nu,\mathbb{R}^2}$, so

$$|\sigma_{\epsilon_l}^{d_l}-\widehat{f}|^2_{3,\Omega_\nu,\mathbb{R}^2}\leq 2|\widehat{f}|^2_{3,\Omega_\nu,\mathbb{R}^2}-2(\sigma_{\epsilon_l}^{d_l},\widehat{f})_{3,\Omega_\nu,\mathbb{R}^2}.$$

However, $\sigma_{\epsilon_l}^{d_l}\overset{\mathrm{H}^3(\Omega_\nu,\mathbb{R}^2)}{\rightharpoonup}\widehat{f}$, consequently
$\forall\varphi\in L^2(\Omega_\nu,\mathbb{R}^2)$, $(\partial^\alpha\sigma_{\epsilon_l}^{d_l},\varphi)_{L^2(\Omega_\nu,\mathbb{R}^2)}\underset{l\to+\infty}{\longrightarrow}(\partial^\alpha\widehat{f},\varphi)_{L^2(\Omega_\nu,\mathbb{R}^2)}$, $\forall\alpha\in\mathbb{N}$, $|\alpha|=3$. Taking $\varphi=\partial^\alpha\widehat{f}$ with $|\alpha|=3$, it yields:
$(\partial^\alpha\sigma_{\epsilon_l}^{d_l},\partial^\alpha\widehat{f})_{L^2(\Omega_\nu,\mathbb{R}^2)}\underset{l\to+\infty}{\longrightarrow}||\partial^\alpha\widehat{f}||^2_{L^2(\Omega_\nu,\mathbb{R}^2)}$ and $(\sigma_{\epsilon_l}^{d_l},\widehat{f})_{3,\Omega_\nu,\mathbb{R}^2}\longrightarrow|\widehat{f}|_{3,\Omega_\nu,\mathbb{R}^2}$.
It follows from the previous inequality that $\lim\limits_{l\to\infty}\|\sigma_{\epsilon_l}^{d_l}-\widehat{f}\|_{\mathrm{H}^3(\Omega_\nu,\mathbb{R}^2)}=0$.

Fourth Step

Assume that $\|\sigma_\epsilon^d-\widehat{f}\|_{\mathrm{H}^3(\Omega_\nu,\mathbb{R}^2)}$ does not tend to 0 when d tends to 0.
It means that there exist a real number $\alpha>0$ and two sequences $(d_k)_{k\in\mathbb{N}}$ and $(\epsilon_k)_{k\in\mathbb{N}}$ such that $d_k\underset{k\to+\infty}{\longrightarrow}0$ and $\epsilon_k=\epsilon(d_k)$ and $\forall k\in\mathbb{N}$,

$$\|\sigma_{\epsilon_k}^{d_k}-\widehat{f}\|_{\mathrm{H}^3(\Omega_\nu,\mathbb{R}^2)}>\alpha. \tag{3.9}$$

Following the same steps as previously done, there exists a subsequence of $\left(\sigma_{\epsilon_k}^{d_k}\right)_{k\in\mathbb{N}}$ that strongly converges to $\widehat{f}$ in $\mathrm{H}^3(\Omega_\nu,\mathbb{R}^2)$, which is in contradiction with (3.9). ∎

3.5. Discretization. We now discretize the variational problem (3.5). To do so, we will use classical notations used in the Finite Element theory (similar to those in [2] and [12]). Let $\mathcal{H}$ be an open bounded subset of $]0,+\infty[$ admitting 0 as accumulation point. Let us recall that the elements of class $\mathrm{C}^{k'}$ can be used for the computation of discrete D^m-splines (in our case $m=3$) with $m \leq k'+1$ (where k' is an integer). Consequently, $(k',m)=(2,3)$ is a satisfactory combination. We also recall that for all $n \in \mathbb{N}$ and for all subsets E of $\mathbb{R}^2$, $Q_l(E)$ denotes the space of the restrictions to E of the polynomial functions over $\mathbb{R}^2$ of degree $\leq l$ with respect to each variable. $\forall h \in \mathcal{H}$, let $(V_h)^2$ be the subspace of $\mathrm{H}^3(\Omega_\nu,\mathbb{R}^2)$ of finite dimension with $(V_h)^2 \circlearrowleft \mathrm{C}^1(\overline{\Omega_\nu},\mathbb{R}^2)$. The reference finite element is the Bogner–Fox–Schmit $\mathcal{C}^2$ rectangle (cf. [12]). It is defined as the following triplet (K,P_K,Σ_K):

- Let $b_{00}=\left(b_{00}^1,b_{00}^2\right)\in\mathbb{R}^2$, $h_1,h_2>0$. $K\subset\Omega_\nu$ is the rectangle with vertices $b_\gamma = b_{00}+\gamma_1 h_1 \vec{e_1}+\gamma_2 h_2 \vec{e_2}$ with $\gamma=(\gamma_1,\gamma_2)\in\mathbb{N}^2$ such that $0\leq\gamma_1\leq 1$ and $0\leq\gamma_2\leq 1$, and $(\vec{e_1},\vec{e_2})$ the canonical basis of $\mathbb{R}^2$.
- $P_K = Q_5(K)$.
- The set of linear mappings Σ_K is defined by: $\Sigma_K=\{v\mapsto\partial^\alpha v(b_\gamma)\,|\,|\alpha|_\infty\leq 2\}$, where, if $\alpha=(\alpha_1,\alpha_2)$, $|\alpha|_\infty=\max(\alpha_1,\alpha_2)$.

The number of degrees of freedom of the Bogner–Fox–Schmit rectangle of class $\mathcal{C}^2$ is thus equal to 36.

The basis functions are defined by $p_\alpha^\gamma(x_1,x_2)=h_1^{\alpha_1}h_2^{\alpha_2}q_{\alpha_1}^{\gamma_1}\left(\dfrac{x_1-b_{00}^1}{h_1}\right)q_{\alpha_2}^{\gamma_2}\left(\dfrac{x_2-b_{00}^2}{h_2}\right)$ with:

$$q_0^0(t)=(1-t)^3(6t^2+3t+1),\ q_1^0(t)=t(1-t)^3(3t+1),\ q_2^0(t)=\frac{1}{2}t^2(1-t)^3$$
$$q_0^1(t)=t^3(6t^2-15t+10),\ q_1^1(t)=t^3(1-t)(3t-4),\ q_2^1(t)=\frac{1}{2}t^3(t-1)^2.$$

We can prove that problem (3.5) is decoupled with respect to each component. Let $(v_q)_{q=1,2}$ be the components of $v\in\mathrm{H}^3(\Omega_\nu,\mathbb{R}^2)$, $((\omega_q^i)^T)_{q=1,2}$ the q^{th} row of ω_i, $\forall i\in\{1,\dots,N\}$, and $\lambda=(\lambda^q)_{q=1,2}$ with $\lambda^q\in\mathbb{R}^l$.
Problem (3.5) can therefore be stated as:

$$\begin{cases}\text{Search for } (\sigma_\epsilon=(\sigma_\epsilon^q)_{q=1,2},\lambda=(\lambda^q)_{q=1,2})\in\mathrm{H}^3(\Omega_\nu,\mathbb{R}^2)\times\mathbb{R}^{2l} \text{ such that}\\ \sigma_\epsilon\in K,\\ \forall v=(v^q)_{q=1,2}\in\mathrm{H}^3(\Omega_\nu,\mathbb{R}^2),\ \forall q\in\{1,2\},\\ \displaystyle\sum_{i=1}^N\langle\nabla\sigma_\epsilon^q(a_i),\nabla v^q(a_i)\rangle_2+\epsilon(\sigma_\epsilon^q,v^q)_{3,\Omega_\nu,\mathbb{R}}+\sum_{i=1}^l\lambda_i^q v^q(b_i)=\sum_{i=1}^N\langle\nabla v^q(a_i),\omega_q^i\rangle_2.\end{cases}\tag{3.10}$$

We solve (3.10) in V_h for $q=1,2$. Let M_h be the dimension of V_h and $\{P_j^h\}_{j=1,\dots,M_h}$ be basis functions (for the sake of clarity, from now on, we use this notation for the basis functions). We denote by $(\sigma_\epsilon^{h,q})_{q=1,2}$ the approximate solution of (3.10) in $(V_h)^2$; $\sigma_\epsilon^{h,q}$ is decomposed into the basis $\{P_j^h\}_{j=1,\dots,M_h}$ as follows:

$$\begin{cases}\forall q=1,2,\\ \exists(\alpha_j^q)_{j=1,\dots,M_h}\in\mathbb{R}\text{ such that}\\ \sigma_\epsilon^{h,q}=\displaystyle\sum_{j=1}^{M_h}\alpha_j^q P_j^h.\end{cases}\tag{3.11}$$

For $q=1,2$, taking successively $v^q=P_k^h$, $k=1,\dots,M_h$ in (3.10), the studied problem becomes:

$$\begin{cases} \text{Search for } \alpha^q\in\mathbb{R}^{M_h} \text{ such that} \\ \sum_{i=1}^{M_h}\alpha_i^q P_i^h(b_j)=\eta_j^q,\ \forall j\in\{1,\cdots,l\}, \\ \forall k=1,\dots,M_h, \\ \sum_{i=1}^{N}\sum_{j=1}^{M_h}\alpha_j^q\langle\nabla P_j^h(a_i),\nabla P_k^h(a_i)\rangle_2+\epsilon\sum_{j=1}^{M_h}\alpha_j^q(P_j^h,P_k^h)_{3,\Omega_\nu,\mathbb{R}}-\sum_{i=1}^{N}\langle\nabla P_k^h(a_i),\omega_q^i\rangle_2 \\ +\sum_{i=1}^{l}\lambda_i^q P_k^h(b_i)=0. \end{cases} \tag{3.12}$$

The numerical problem amounts to solving two decoupled sparse linear systems of dimension $(M_h+l)\times(M_h+l)$ which can be written by means of matrices A^h, B^h and R^h,

$$A^h=\left(\frac{\partial P_j^h}{\partial x_1}(a_i)\right)_{\substack{1\le i\le N,\\ 1\le j\le M_h}},\ B^h=\left(\frac{\partial P_j^h}{\partial x_2}(a_i)\right)_{\substack{1\le i\le N,\\ 1\le j\le M_h}}\in\left(\mathcal{M}_{N\times M_h}(\mathbb{R})\right)^2,$$

$$R^h=\left((P_j^h,P_i^h)_{3,\Omega,\mathbb{R}}\right)_{1\le i\le M_h,1\le j\le M_h}\in\mathcal{M}_{M_h\times M_h}(\mathbb{R}).$$

Both systems are written in the following way:

$$\begin{cases} \left((A^h)^TA^h+(B^h)^TB^h+\epsilon R\right)\alpha^q+(P^h)^T\lambda^q=\xi_q, \\ \text{with } P^h\alpha^q=\eta^q,\ \forall q\in\{1,2\}, \end{cases} \tag{3.13}$$

where $P^h=\left(P_j^h(b_i)\right)_{\substack{1\le i\le l,\\ 1\le j\le M_h}}\in\mathcal{M}_{l\times M_h}(\mathbb{R})$ and $\xi_q=\left(\sum_{i=1}^{N}\langle\nabla P_k^h(a_i),\omega_q^i\rangle_2\right)_{1\le k\le M_h}$. We group the unknown α^q and λ^q in a single unknown vector, and we write the system as a matrix equation of the form:

$$\kappa^h\left\{\begin{array}{c} \\ M_h \\ \\ l \end{array}\right.\overset{\begin{array}{cc} M_h & l \end{array}}{\left(\begin{array}{c|c} (A^h)^TA^h+(B^h)^TB^h+\epsilon R & (P^h)^T \\ \hline P^h & 0 \end{array}\right)}\quad\left(\begin{array}{c}\alpha^q\\ \hline \lambda^q\end{array}\right)=\left(\begin{array}{c}\xi^q\\ \hline \eta^q\end{array}\right)$$

REMARK 3.9. A result of convergence analogous to the one in Theorem 3.8 can be obtained in the discrete setting.

REMARK 3.10. The matrix κ^h of the system is symmetric indefinite.

REMARK 3.11. In practice, the interpolation conditions are set on the boundary nodes of the finite element mesh. In this case, we have the following result:

PROPOSITION 3.12. *Matrix κ^h is nonsingular.*

Proof. For the sake of clarity, we denote by C^h the matrix $C^h = (A^h)^T A^h + (B^h)^T B^h + \epsilon R$. The proof is based on Lemma 16.1 of [33] that states that if Z is a basis for the null space of P^h and if the reduced Hessian $Z^T C^h Z$ is positive definite and $\left(P^h\right)^T$ has full rank, then κ^h is nonsingular.

As the interpolation conditions are set on the boundary of the finite element mesh, the columns of $\left(P^h\right)^T$ are made of l independent vectors of the canonical basis of $\mathbb{R}^{M_h}$, so $\left(P^h\right)^T$ has full rank. More precisely, if the column of index p of $\left(P^h\right)^T$ denoted by $\left(P^h\right)^T_p$ is related to node $q(p)$ of the finite element mesh, one has: $\left(P^h\right)^T_{j,p} = \begin{vmatrix} 1 \text{ if } j = 9(q-1)+1, \\ 0 \text{ otherwise} \end{vmatrix}$, $j \in \{1, \cdots, M_h\}$.
The columns $(Z_1, \cdots, Z_{M_h - l})$ of Z are thus made of the $M_h - l$ (independent) vectors of the canonical basis of $\mathbb{R}^{M_h}$ orthogonal to the columns of $\left(P^h\right)^T$.

The matrix C^h is semi-positive definite. Indeed, $\forall \alpha \in \mathbb{R}^{M_h}$, $\alpha^T C^h \alpha = a(v^h, v^h) \geq 0$ with $v^h = \sum_{j=1}^{M_h} \alpha_j P^h_j$. From what was previously done, the quantity $a(v^h, v^h)$ vanishes when v^h is a constant c_1, which corresponds to $\alpha = (\alpha_j)_{j=1}^{M_h}$ such that $\alpha_j = \begin{vmatrix} c_1 \text{ if } j = 1 + 9s,\ s \in \left\{0, \cdots, \frac{M_h}{9} - 1\right\}, \\ 0 \text{ otherwise} \end{vmatrix}$. In particular, the vector $\xi \in \mathbb{R}^{M_h}$ defined by $\xi_j = \begin{vmatrix} 1 \text{ if } j = 1 + 9s,\ s \in \left\{0, \cdots, \frac{M_h}{9} - 1\right\}, \\ 0 \text{ otherwise} \end{vmatrix}$ is not spanned by $(Z_1, \cdots, Z_{M_h - l})$. Let us now take $X \in \mathbb{R}^{M_h - l} \setminus \{0_{\mathbb{R}^{M_h - l}}\}$. It is clear that $ZX \notin \operatorname{span}(\xi)$ so $X^T Z^T C^h Z X > 0$, which achieves the proof. ∎

A large variety of methods can be found in the literature to solve the considered linear systems: null-space methods ([17, 3]), direct solvers ([9]), the classical Uzawa algorithm ([4]), the inexact Uzawa algorithm ([16]), splitting schemes ([15]), augmented Lagrangian approach ([18]). In our application, we use the diagonal pivoting method due to Bunch and Parlett ([9]) which computes a permutation P such that $PAP^T = LDL^T$ —when solving a linear system whose symmetric matrix is A—where D is a direct sum of 1 by 1 and 2 by 2 pivot blocks and L is unit lower triangular (see also [19]). P is chosen so that the entries in the unit lower triangular L satisfy $|l_{ij}| \leq 1$. This factorization involves $\frac{n^3}{3}$ flops and once computed can be used to solve $Ax = b$ with $\mathcal{O}(n^2)$ work.

Remark 3.13 (Extension of the algorithm to the 3D case). The main brake to the straight extension of the model to 3D is the phase of identification of subdomains (in practice small cubes) where the computations need to be done. (In 2D, visual inspection suffices to determine these regions.) The semi-automation of this process, based on segmentation techniques, is a project in progress. The idea is to work with the 3D images of the discrete Jacobians and to partition the images into two smooth regions: a region for which the discrete Jacobians are greater than a defined threshold and a region for which they are lower (region that thus needs to be processed). This binary partition of the data can be performed using a Chan–Vese like ([10]) segmentation criterion in a level set framework. This step is done for each discrete Jacobian. The regions to be processed are thus localized and are embedded in cubes. The derivation of the topology-preserving conditions in the 3D case is quite analogous to the 2D case. We impose that the 8 corner Jacobians are positive (see [25] for justifications). The Jacobian $J_\alpha(x, y, z)$ is now a polynomial of degree 3 in α but the method, as in the 2D case, amounts to studying the roots of polynomials, here of degree 3. The theoretical results in the reconstruction stage

hold in three dimensions. The numerical problem consists in solving three decoupled sparse linear systems of dimension $(M_h+l)\times(M_h+l)$ but this time there are 3^3 basis functions per node so $M_h=\dim V_h=3^3\times$ number of mesh nodes. The basis functions are still obtained by tensor product from the 1D case and the system matrix structure is the same, except that the block (1,1) is of the form $(A^h)^TA^h+(B^h)^TB^h+(C^h)^TC^h+\epsilon R$, with $C_h=\left(\frac{\partial P_j^h}{\partial x_3}(a_i)\right)_{\substack{1\le i\le N,\\ 1\le j\le M_h}}$. The optimization computational tools are the same as the ones in Section 4. Some very preliminary experiments have been made on cubes of size $36\times36\times36$ and the computational time decreases to 23 seconds.

4. Numerical experiments

In the sequel, we provide numerical simulations. Classically, in the D^m-spline setting, parameter ϵ balancing the semi-norm is set to 10^{-6}. (There also exist methods for an automatic choice of ϵ mainly based on statistical considerations as the generalized cross-validation and the generalized maximum likelihood methods, see [13] and [20].) From our experience, we have realized that it suffices to fix the value ϵ in a neighborhood of 10^{-6} to produce satisfactory results. Besides, the method proves to be not too sensitive to the choice of this parameter. That is why we did not resort to the generalized cross-validation method to set parameter ϵ. Owing to the fact that the proposed algorithm calls basic linear algebra functions such that transposing matrices, summing matrices, multiplying matrices or solving linear systems, it appeared relevant to use LAPACK and Basic Linear Algebra Subprogram routines (official websites: `http://www.netlib.org/blas/` and `http://www.netlib.org/lapack/`). BLAS is a corpus of routines that provides standard building blocks for performing basic vector and matrix operations. LAPACK (designed at the outset to exploit BLAS routines) provides routines for solving systems of linear equations among others. For each subdomain Ω_ν, $\nu\in\{1,\cdots,\mathcal{N}\}$, we obtain two disconnected linear systems to be solved with the same matrix. Our resorting to BLAS/LAPACK thus seems apposite. We particularly focused on the *dsysv* function provided by the software package LAPACK which computes the solution of a real system of linear equations $AX=B$ (where A is an N-by-N symmetric matrix and X and B are N-by-$NRHS$ matrices) using the diagonal pivoting method. Also, we capitalized on the *dgemm* routine to perform matrix-matrix operations. The computations on each subdomain Ω_ν being independent, the use of OpenMP appeared relevant. The OpenMP Application Program Interface supports multi-platform shared-memory programing in C/C++ and Fortran on all architectures (see the official website `http://openmp.org/wp/`). In the sequel, the OMP_NUM_THREADS environment variable sets the number of threads that the program uses. The MKL_NUM_THREAD environment variable enables to MKL threading inside the threading of the application. For our configuration, the maximal number of threads is equal to 12.

4.1. First example: a slice of the brain. In the first application, the goal is to map a disk to a slice of the brain (courtesy of the Laboratory of Neuro-Imaging, School of Medicine, University of California) defined on the same image domain (size 120 × 190), while preserving topology (see Figure 4.1 (a)). In this example, we only aim to align the shapes, i.e., the contour of the slice of brain with the boundary of the disk (whatever the genus of the shapes is).

When applying the combined segmentation/registration model developed in [27] without regridding steps, we obtain a deformation field exhibiting two regions with overlaps as depicted in Figure 4.1 (b)–(d). If we merely apply the method developed in

Experiment	Number of regions exhibiting overlaps	OMP_NUM_THREADS	MKL_NUM_THREADS	Computation time	Depleting factor
Slice of the brain 1. Size 120×190	2 regions: Size 30×30 & Size 80×40	2	6	0.63 s	80
Slice of the brain 2. Size 61×81	2 regions: Size 53×61 & Size 21×61	2	6	0.66 s	4
Disks. Size 100×100	2 regions: Size 50×50 & Size 50×50	2	6	0.52 s	6.9

Table 4.1: Summary of the various parameters involved in the experiments.

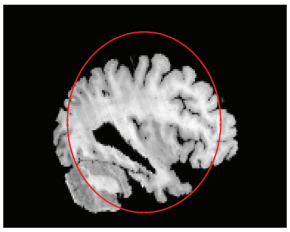

(a) Reference image and boundary (in red) of the disk constituting the Template image.

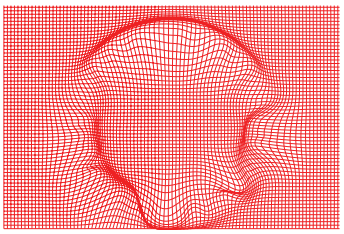

(b) Obtained global deformation field when topology preservation is notenforced.

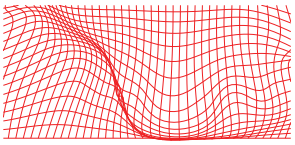

(c) Zoom on the first region exhibiting overlaps.

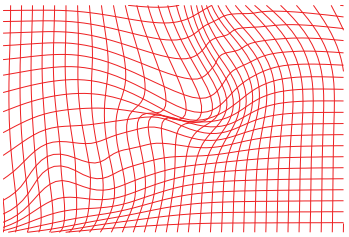

(d) Zoom on the second region exhibiting overlaps.

Fig. 4.1: *Example of the slice of the brain: obtained uncorrected deformation field.*

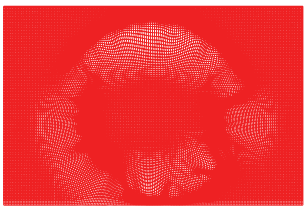

(a) Global obtained deformation field.

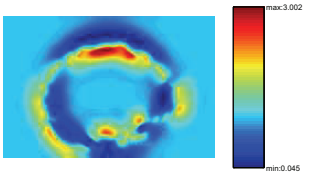

(b) Jacobian determinant of the obtained deformation field.

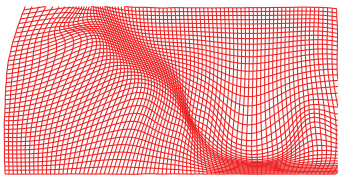

(c) Zoom on the corrected first region: $\min(J_{ff}) = 0.20$, $\min(J_{fb}) = 0.21$, $\min(J_{bf}) = 0.17$ and $\min(J_{bb}) = 0.19$.

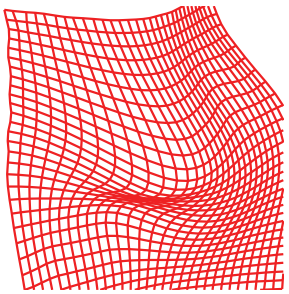

(d) Zoom on the corrected second region: $\min(J_{ff}) = 0.13$, $\min(J_{fb}) = 0.19$, $\min(J_{bf}) = 0.21$ and $\min(J_{bb}) = 0.23$.

Fig. 4.2: *Example of the slice of the brain: obtained orientation-preserving deformation field.*

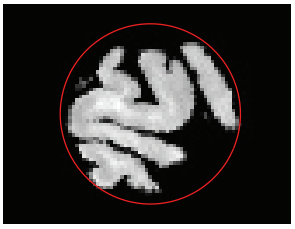

(a) Boundary of the disk constituting the Template image superimposed on the Reference image.

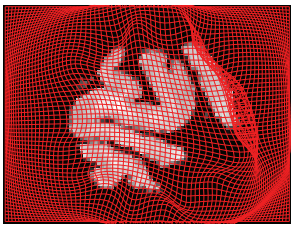

(b) Obtained global deformation field when topology preservation is not enforced.

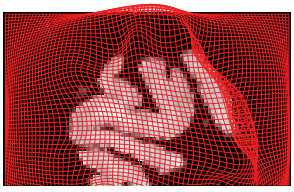

(c) Zoom on the first region exhibiting overlaps.

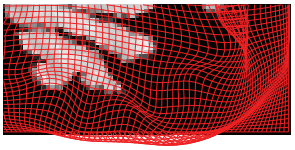

(d) Zoom on the second region exhibiting overlaps.

Fig. 4.3: *Example of the slice of the brain with large deformations: obtained uncorrected deformation field.*

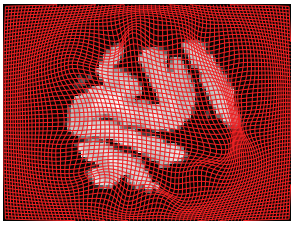

(a) Global obtained deformation field.

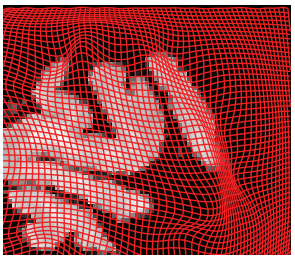

(b) Zoom on the corrected first region: $\min(J_{ff}) = 0.21$, $\min(J_{fb}) = 0.20$, $\min(J_{bf}) = 0.21$ and $\min(J_{bb}) = 0.20$.

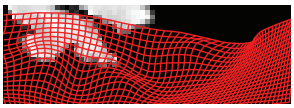

(c) Zoom on the corrected second region: $\min(J_{ff}) = 0.24$, $\min(J_{fb}) = 0.19$, $\min(J_{bf}) = 0.31$ and $\min(J_{bb}) = 0.30$.

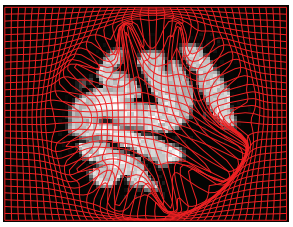

(d) Obtained result with Christensen et al's regridding technique ([11])

Fig. 4.4: *Example of the slice of the brain with large deformations: obtained orientation-preserving deformation field.*

[26] (which consists in applying the correction/reconstruction algorithm on the whole image domain with global condition on the deformation component means), the execution time reaches 50.9 seconds. By applying our proposed method, the computational time drops to 0.63 second, which means a depletion by a factor 80. We display the obtained topology-preserving deformation fields together with the values of the discrete Jacobians in Figure 4.2.

4.2. Second example: brain mapping. A second example still dedicated to brain mapping (courtesy of the Laboratory of Neuro-Imaging, School of Medicine, University of California) is given in Figure 4.3, demonstrating the ability of the method to handle high-magnitude deformations. The goal is to register a disk to the outer boundary of the brain, both defined on the same image domain of size 61×81, while maintaining topology. When applying the combined segmentation/registration model developed in [27] without regridding steps, we obtain a deformation field exhibiting two regions with overlaps as depicted in Figure 4.3.

Applying the algorithm developed in [26] on the whole image domain yields a computational time of 2.62 seconds. By comparison, when the proposed algorithm is applied simultaneously on the two regions depicted in Figure 4.3(c) and Figure 4.3(d) (respectively of size 53×61 and 21×61), the computational time drops to 0.66 second, which means a depletion by a factor 4. We display the obtained topology-preserving deformation field together with the values of the discrete Jacobians in Figure 4.4. With Christensen et al.'s regridding technique ([11]) (in the spirit of our methodology, we compared what was comparable, namely the topology-preserving method: we applied Christensen et al.'s regridding technique within the registration model [26]), 3 regridding steps were necessary: the transformation was considered as admissible if the Jacobian exceeded 0.075. Unfortunately, at the end of the process, the minimum of the Jacobian of the transformation is equal to -0.5288 and overlaps are still visible on the grid (see Figure 4.4) (d).

4.3. Third example: the disks. Another application involving large deformations is provided in Figure 4.5 and is similar to an application given in [27] in the case of topology-preserving segmentation. The synthetic Reference image represents two disks. The Template image, which is defined on the same image domain (100×100), is made of a black ellipse such that when superimposed on the Reference image its boundary encloses the two disks (see Figure 4.5 (a)). The application of the combined segmentation-registration process alone yields two regions exhibiting overlaps (Figure 4.5(b)): the upper part of the image including the upper disk (size 50×50) and the lower part of the image containing the lower disk (size 50×50). We thus propose to apply our proposed algorithm on each region independently. The computational time drops to 0.52 second, which means a depletion by a factor 6.9 in comparison to the computational time inherent to the application of the method [26] on the whole domain. We display the obtained topology-preserving deformation fields together with the values of the discrete Jacobians in Figure 4.5 (c) and Figure 4.5 (d).

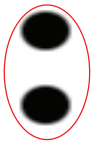

(a) Reference image and boundary of the ellipse constituting the Template image superimposed.

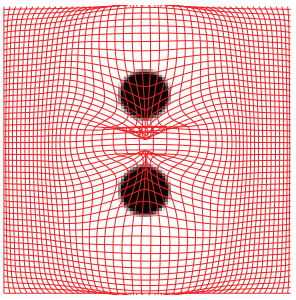

(b) Obtained global deformation field when topology preservation is not enforced.

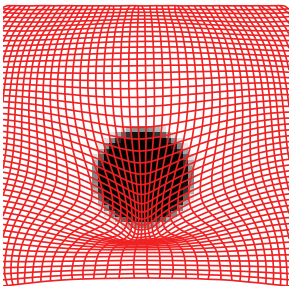

(c) Corrected first region: $\min\left(J_{ff}\right) = 0.06$, $\min\left(J_{fb}\right) = 0.08$, $\min\left(J_{bf}\right) = 0.09$ and $\min\left(J_{bb}\right) = 0.11$.

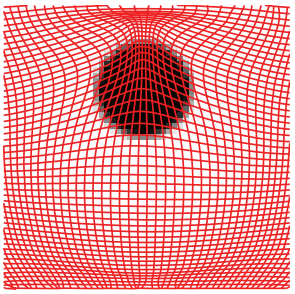

(d) Corrected second region: $\min\left(J_{ff}\right) = 0.33$, $\min\left(J_{fb}\right) = 0.31$, $\min\left(J_{bf}\right) = 0.35$ and $\min\left(J_{bb}\right) = 0.29$.

Fig. 4.5: *Example of the disks.*

REFERENCES

[1] R.A. Adams, *Sobolev Spaces*, Academic, Boston, MA, 1975.

[2] R. Arcangéli, M.C. López de Silanes, and J.J. Torrens, *Multidimensional minimizing splines. Theory and applications*, Grenoble Sciences, Kluwer Academic Publishers, Boston, MA, 2004.

[3] M. Arioli and L. Baldini, *A backward error analysis of a null space algorithm in sparse quadratic programming*, SIAM J. Matrix Anal. Appl., 23, 425–442, 2001.

[4] K. Arrow, L. Hurwicz, and H. Uzawa, *Studies in Nonlinear Programming*, Stanford University Press, Stanford, 1958.

[5] J. Ashburner, J.L.R. Andersson, and K.J. Friston, *High-dimensional image registration using symmetric priors*, Neuroimage, 9, 619–628, 1999.

[6] J. Ashburner and K.J. Friston, *Voxel-based morphometry: the methods*, Neuroimage, 11, 805–821, 2000.

[7] J. Ashburner, P. Neelin, D.L. Collins, A. Evans, and K.J. Firston, *Incorporating prior knowledge into image registration*, Neuroimage, 6, 344–352, 1997.

[8] H. Brezis, *Analyse Fonctionelle. Théorie et Applications*, Dunod, Paris, 2005.

[9] J.R. Bunch and B.N. Parlett, *Direct methods for solving symmetric indefinite systems of linear equations*, SIAM J. Numer. Anal., 8, 639–655, 1971.

[10] T. Chan and L. Vese, *Active contours without edges*, IEEE Trans. Image Process., 10, 266–277, 2001.

[11] G.E. Christensen, R.D. Rabitt, and M.I. Miller, *Deformable templates using large deformation kinematics*, IEEE Trans. Imag. Process., 10, 1435–1447, 1996.

[12] P.G. Ciarlet, *The Finite Element Method for Elliptic Problems*, North Holland, Amsterdam, The Netherlands, 1978.

[13] P. Craven and G. Wahba, *Smoothing noisy data with spline functions*, Numer. Math., 31, 377–403, 1979.
[14] M. Droske and M. Rumpf, *A variational approach to non-rigid morphological registration*, SIAM J. Appl. Math., 64, 668–687, 2004.
[15] N. Dyn and W.E. Ferguson, *The numerical solution of equality-constrained quadratic programming problems*, Math. Comput., 41, 165–170, 1983.
[16] H.C. Elman and G.H. Golub, *Inexact and preconditioned Uzawa algorithms for saddle point problems*, SIAM J. Numer. Anal., 31, 1645–1661, 1994.
[17] R. Fletcher and T. Johnson, *On the Stability of Null-Space Methods for KKT Systems*, tech. report, University of Dundee, Department of Mathematics and Computer Science, Dundee, UK, 1995.
[18] G.H. Golub and C. Greif, *On solving block-structured indefinite linear systems*, SIAM J. Sci. Comput., 24, 2076–2092, 2003.
[19] G.H. Golub and C.F. Van Loan, *Matrix Computations*, Fourth Edition, Johns Hopkins University Press, Baltimore, 2013.
[20] C. Gu and G. Wahba, *Minimizing GCV/GML scores with multiple smoothing parameters via the newton method*, SIAM J. Sci. Stat. Comput., 12, 383–398, 1991.
[21] E. Haber and J. Modersitzki, *Numerical methods for volume preserving image registration*, Inverse Probl., 20, 1621–1638, 2004.
[22] E. Haber and J. Modersitzki, *Image registration method with guaranteed displacement regularity*, Int. J. Comput. Vision, 71, 361–372, 2007.
[23] X. Han, C. Xu, U. Braga-Neto, and J.L. Prince, *Topology correction in brain cortex segmentation using a multiscale, graph-based algorithm*, IEEE Trans. Med. Imag., 21, 109–121, 2002.
[24] X. Han, C. Xu, U. Braga-Neto, and J.L. Prince, *A topology preserving geometric deformable model and its application in brain cortical surface reconstruction*, in Geometric Level Set Methods in Imaging, Vis., Graph., Stanley Osher and Nikos Paragios, Eds., New York: Springer-Verlag, 2003.
[25] B. Karaçali and C. Davatzikos, *Estimating topology preserving and smooth displacement fields*, IEEE Trans. Med. Imag., 23, 868–880, 2004.
[26] C. Le Guyader, D. Apprato, and C. Gout, *On the construction of topology-preserving deformation fields*, IEEE Trans. Image Process., 21, 1587–1599, 2012.
[27] C. Le Guyader and L. Vese, *A combined segmentation and registration framework with a nonlinear elasticity smoother*, Computer Vision and Image Understanding, 115, 1689–1709, 2011.
[28] J. Modersitzki, *Numerical Methods for Image Registration*, Oxford University Press, 2004.
[29] J. Modersitzki, *FAIR: Flexible Algorithms for Image Registration*, Society for Industrial and Applied Mathematics (SIAM), 2009.
[30] O. Musse, F. Heitz, and J.P. Armspach, *Topology preserving deformable image matching using constrained hierarchical parametric models*, IEEE Trans. Image Process., 10, 1081–1093, 2001.
[31] J. Nečas, *Les méthodes directes en théorie des équations elliptiques*, Masson, Paris, 1967.
[32] V. Noblet, C. Heinrich, F. Heitz, and J.P. Armspach, *3-D deformable image registration: a topology preservation scheme based on hierarchical deformation models and interval analysis optimization*, IEEE Trans. Image Process., 14, 553–566, 2005.
[33] J. Nocedal and S.J. Wright, *Numerical Optimization*, Springer, New York, 1999.
[34] I. Yanovsky, P.M. Thompson, S. Osher, and A.D. Leow, *Topology preserving log-unbiased nonlinear image registration: Theory and implementation*, in Proc. IEEE Conf. Comput. Vis. Pattern Recognit., 1–8, 2007.